ADVANCED FUNCTIONAL MATERIALS
www.afm-journal.de

www.MaterialsViews.com

Molecular Mechanism of Specific Recognition of Cubic Pt Nanocrystals by Peptides and of the Concentration-Dependent Formation from Seed Crystals

Hadi Ramezani-Dakhel, Lingyan Ruan, Yu Huang, and Hendrik Heinz**

Metal nanocrystals enable new functionality in sensors, biomarkers, and catalysts while mechanisms of shape-control in synthesis remain incompletely understood. This study explains mechanisms of biomolecule recognition and ligand-directed growth of cubic platinum nanocrystals in atomic detail using molecular dynamics simulation (MD), synthesis, and characterization. Peptide T7 is shown to selectively recognize {100} bounded nanocubes through preferential adsorption near the edges as opposed to facet centers. Spatial preferences in peptide binding are related to differences in the binding of water molecules and conformational matching of polarizable atoms in the peptide to {100} epitaxial sites. Changes in peptide concentration also have profound impact on attraction versus repulsion on a given surface. As an example, the selective synthesis of cubes in the presence of peptide T7 demonstrates that only intermediate T7 concentration leads to high yield. High-resolution transmission electron microscopy (HRTEM) shows concentration-dependent changes in crystal shape, yield, and size. Large-scale MD simulations explain associated differences in facet coverage and in adsorption energies of T7 peptides on cuboctahedral seed crystals, supporting a growth mechanism of adatom deposition. A similar analysis using a different peptide S7 is presented as well. Emerging computational opportunities to predict ligand binding to metal nanocrystals and rationalize growth preferences are summarized.

1. Introduction

The functionality of metal nanostructures in sensors, therapeutics, catalysts, optical, and electronic devices is determined by their shape, size, and surface modification.[1] Short polymers of naturally occurring amino acids have been employed as efficient regulating agents to program nanocrystal shape via recognition of crystallographic facets.[2–4] It is believed that differences in the relative growth rate of facets in the presence of selective ligands cause the evolution of a specific crystal shape.[2,5–7] The mechanisms of the interactions at the interface of biomolecules and nanoscale metal substrates, however, remain difficult to examine due to the inaccessibility of the interfaces to most of the advanced detection techniques and the complexity of the interactions.[2,7,8] Computational methods have been employed to overcome such limitations by probing binding conformations and the binding strength of biomolecules to metal surfaces.[9–18] The range of methods includes quantum mechanical simulations, lattice energy relaxation, lattice dynamics, molecular dynamics, and Monte Carlo methods. In aqueous solution, peptide binding to clean metal surfaces involves predominantly noncovalent interactions, while complexation of metal precursor ions by certain residues (e.g., His) and participation in reduction reactions (e.g., Tyr) can also influence reaction kinetics.

Molecular dynamics (MD) simulations using the CHARMM-METAL, CVFF-METAL,[13,15] and the GoIP (for Au only) force fields[19] have revealed significant details.[10,15,16] Facet-specific interactions of ligands with precious metal surfaces are mainly driven by soft epitaxy and contributions from induced charges. Soft epitaxy involves the coordination of polarizable atoms in the ligands (e.g., O, N, C) with epitaxial sites (also called hollow sites) as well as with top sites on the metal surface in competition with oxygen atoms of water molecules.[14–16,20] Coordination of epitaxial sites is thereby preferred over coordination of top-layer atoms, and the computed adsorption strength correlates with the number of such contacts between the peptide and the metal surface (Figures S1 and S2, Supporting Information).[14,15,20] The associated geometry and strength of adsorption[15,16] are consistent with abundant experimental data, including Low Energy Electron Diffraction (LEED) for organic over-layers on metal surfaces (Figure S1, Supporting Information),[21] binding preferences of various ligands to {100} and {111} facets according to data from phage display, as well as measured binding energies.[10,14–16,18,20–29] Evidence from phage display, for example, has shown the selection of {111} facets

H. Ramezani-Dakhel, Prof. H. Heinz
University of Akron
Department of Polymer Engineering
Akron, OH 44325, USA
E-mail: hendrik.heinz@uakron.edu
L. Ruan, Prof. Y. Huang
University of California
Department of Materials Science and Engineering
Los Angeles, CA 90095, USA
E-mail: yhuang@seas.ucla.edu
Prof. Y. Huang
University of California
California NanoSystems Institute
Los Angeles, CA 90095, USA

DOI: 10.1002/adfm.201404136

by phenyl rings as observed in MD simulation,[16,20] and the relative binding strength of all twenty amino acids has been reproduced by computer simulations.[15] Laboratory observations of strong binding of the same peptides to Ag, Au, Pd, and Pt surfaces also support a soft epitaxial binding mechanism.[20,24,30,31] A secondary contribution to peptide binding is also the attractive polarization of the metal surface by induced charges. This contribution gains relevance in the presence of ionic groups and can become dominant for the adsorption of ionic liquids.[10,27]

Many peptides are strongly attracted to {111} surfaces and approach the metal surface without a water interlayer (<0.3 nm distance).[20,27,29] On {100} surfaces, peptide attraction is typically an order of magnitude weaker and a water interlayer often remains between metal surface and peptide even in case of attraction. Trends in nanoparticle stabilization as a function of size and surface topography, as well as specific ligand binding constants have also been explained by MD simulation and soft epitaxy.[4,14] For example, decreased attraction of peptides and proteins to nanoparticles of smaller size, especially in the range from 10 to 2 nm, as experimentally observed by various groups,[23,28] is related to the range of intermolecular interactions (<2 nm), the presence of more {100} facets than {111} facets on smaller nanoparticles, as well as challenges in conformational adaptation of peptides to higher curvature for small nanoparticle size.[14]

Previous results, experimental and computational, therefore provide understanding of binding configurations and adsorption energies of single peptides on even and shaped surfaces in aqueous solution. Nevertheless, computational methods to date have been mainly applied to single peptides on extended facets. This contribution steps forward with an analysis of the recognition of single and multiple peptides on nanocrystals of different shape in aqueous solution, as well as the elucidation of relationships to the preferred shape, yield, and size of nanocrystals in peptide-directed growth. Specifically, we analyze the selective recognition and synthesis of Pt nanocubes in the presence of peptide T7 (Acyl-TLTTLTN-Amide), and compare the results to different recognition and growth mechanisms in the presence of peptide S7 (Acyl-SSFPQPN-Amide). Through the combination of experiment and all-atom MD simulation, this work also demonstrates that simulation methods are becoming viable tools to elucidate mechanisms of facet recognition and growth of nanostructures of realistic size, including various shapes and sizes up to 100 nm as well as peptide ligands in variable concentration.

The amino acid sequence of peptide T7 (Acyl-TLTTLTN-Amide) was initially identified for specific binding to near-cubic platinum nanocrystals terminated by {100} facets using phage display techniques.[2] Interestingly, the same peptide was not significantly attracted to infinite {100} surfaces. Peptide T7 was nevertheless found to function as a regulating agent to direct the formation of cubic nanocrystals in reductive synthesis, whereby high yield could only be achieved at intermediate peptide concentration. In contrast, another peptide S7 forms tetrahedral nanocrystals across a wide range of concentration in contact with the same platinum seed crystals.

The outline of this paper is as follows. Section 2 proceeds with the results and discussion. Section 3 contains conclusions and Section 4 provides a summary of methods. Additional figures, details of simulations, experiments, and limitations are documented in the Supporting Information (Sections S1 to S4).

2. Results and Discussion

This section describes the mechanisms of selective peptide recognition and crystal growth, and is divided into six subsections. The first three subsections explain the specific recognition of Pt nanocubes by single T7 peptides, specific interactions of single T7 and S7 peptides with Pt cuboctahedral seed crystals, as well as the influence of peptide concentration on facet preferences. The subsequent three subsections describe the mechanism of formation of cubes from cuboctahedral seed crystals as a function of T7 peptide concentration, regulation of nanocrystal shape by a different peptide S7 and thermodynamic stability, as well as emerging simulation capabilities and their relation to laboratory tests.

2.1. Specific Recognition of Platinum Cubes by Single T7 Peptides in Solution

Peptide T7 was identified through phage display to possess a highly specific affinity to platinum cubes at low concentration[2] while no specific attraction to extended {100} surfaces was observed. To explain the specific affinity, adsorption of a single T7 peptide was examined on extended platinum {100} surfaces, cubic nanocrystals, cuboctahedral seeds (**Figure 1**), as well as on extended platinum {111} surfaces (Figure S3, Supporting Information) in aqueous solution using large-scale parallel molecular dynamics simulations. Atoms in the peptide backbone and in the side chains coordinate with both epitaxial and top sites over time. On extended platinum {100} surfaces in aqueous solution, T7 tends to desorb with a positive energy $+13 \pm 1$ kcal mol^{-1} (Figure 1a,b). The peptide is less attracted to surface sites than the competing water molecules, tested by independent simulation setups with adsorbed and desorbed start configurations. Representative configurations in the side and top view show an interlayer of water between the peptide and the surface, and only few atoms in the side chains of the peptide are in direct contact with the metal surface (Acyl, T2, and L2) (Figure 1a,b). Previous studies of binding of other peptides to {100} surfaces of Au, Pd, and Pt[15,16,20] have similarly shown repulsion or weak attraction. The concatenated geometry of the peptide molecule often hinders a complimentary fit to the quadratic pattern of epitaxial sites with a spacing of ≈2.77 Å and, as a result, oxygen atoms in flexible water molecules are attracted with a higher propensity than the peptides. The preference of water molecules in the condensed state toward epitaxial (hollow) sites versus top sites is still debated since experimental evidence remains unavailable.[13,17,27] Thereby, the actual preference has little impact on the results reported here (Section S2.3, Supporting Information).

Earlier experimental and modeling studies also indicate that the overall attraction of water versus peptide depends on the size of the nanoparticles, especially in the 1 to 10 nm range, and changes remarkably near the edges of metal

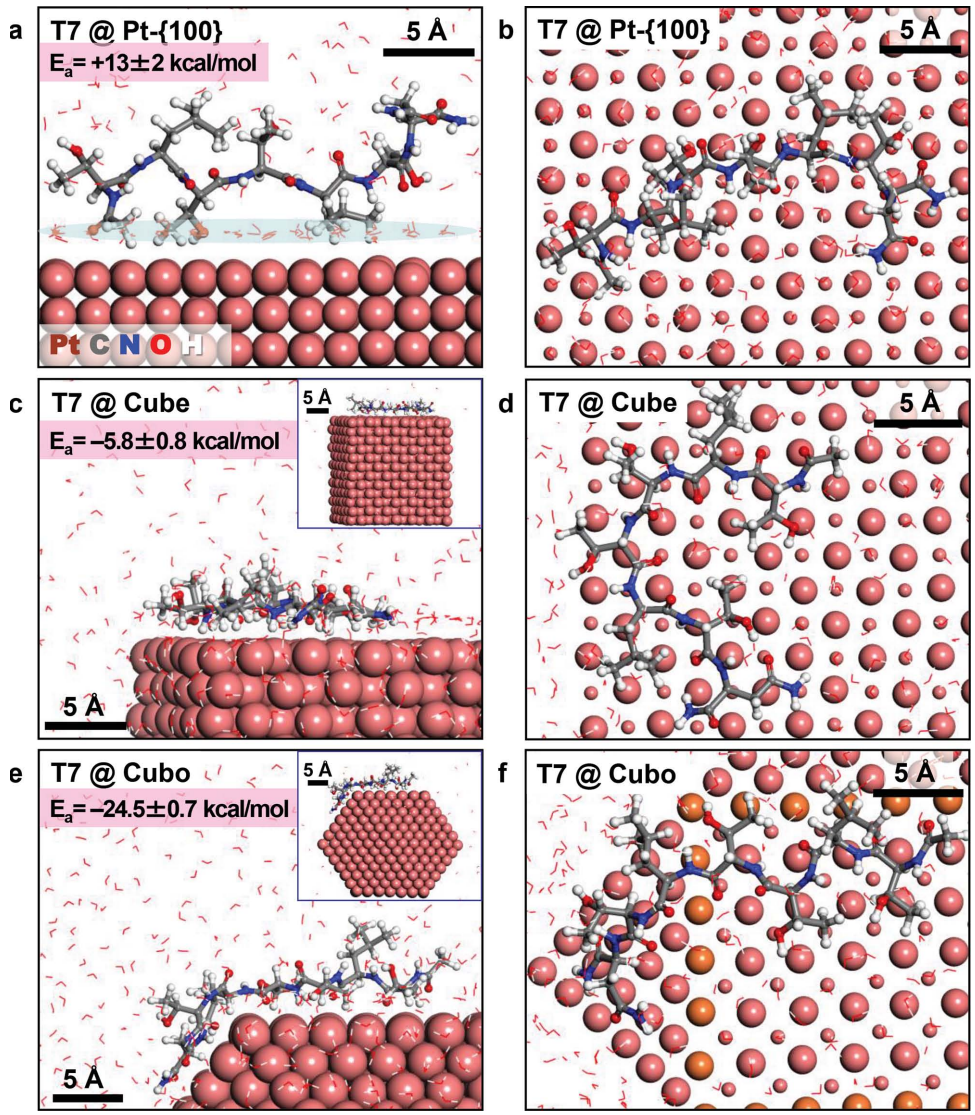

Figure 1. Differences in average binding conformation of a single peptide T7 on extended Pt {100} surfaces, cubes, and cuboctahedra according to molecular dynamics simulation. a,b) Representative configuration on an extended {100} surface in side and top view. Water molecules form a strongly adsorbed interlayer of low mobility between the metal surface and the peptide (highlighted in panel a). The adsorption energy of T7 is positive and a few direct contacts of peptide side chains with the metal surface are found (Acyl, T2, and L2 in the highlighted area). c,d) Representative configuration on a cubic platinum nanoparticle in side and top view. The peptides adsorb favorably near the edge where water molecules are weakly bound and mobile. The peptides thus replace water molecules in the edge area, in contrast to the center of the facets, and nearly all residues interact directly with the surface (see inset in panel c from a different perspective, in which water molecules were removed for visual clarity). The top view (d) shows the exceptional fit of C, N, and O atoms in T7 to about twenty epitaxial sites. Some top sites are also coordinated. e,f) Representative configurations on a cuboctahedron of ≈2 nm side length in side and top view. T7 coordinates mainly with epitaxial sites near the edges of {100} and {111} facets. The major portion of the peptide is adsorbed to the edge of the {100} facet on time average and the adsorption energy is lower (larger negative value) compared to the cube due to simultaneous strong interaction to {111} facets.

surfaces.[14,23,28,31,32] These dependencies can be explained by local changes in the surface potential, which is proportional to the number of metal atoms in the vicinity of a probe molecule.[14] Accordingly, the interaction of single T7 peptides with cubic nanocrystals was found to be strongly location-dependent (Figure 1c,d). Direct surface contact occurs near the edges of {100} facets, accompanied by significant reduction in conformational flexibility and notable adsorption of –5.8 ± 0.8 kcal mol^{-1}. The average distance of alpha-carbon atoms in the peptide from the top atomic layer of cubic Pt is then only 3.5 Å, in contrast to 6.4 Å on the extended {100} surface. Peptide attraction near the edges is thus remarkably opposite to desorption on extended {100} surfaces. In addition, the average adsorbed conformation reveals an exceptional fit of polarizable C, N, and O atoms in peptide T7 to approximately twenty epitaxial sites in the characteristic square pattern (Figure 1d). The high degree of molecular match is far better than for other peptides previously analyzed on Au, Pd, and Pt {100} surfaces.[14,16,20] This near-perfect fit of a single T7 molecule is therefore consistent with the original combinatorial selection of this peptide sequence against

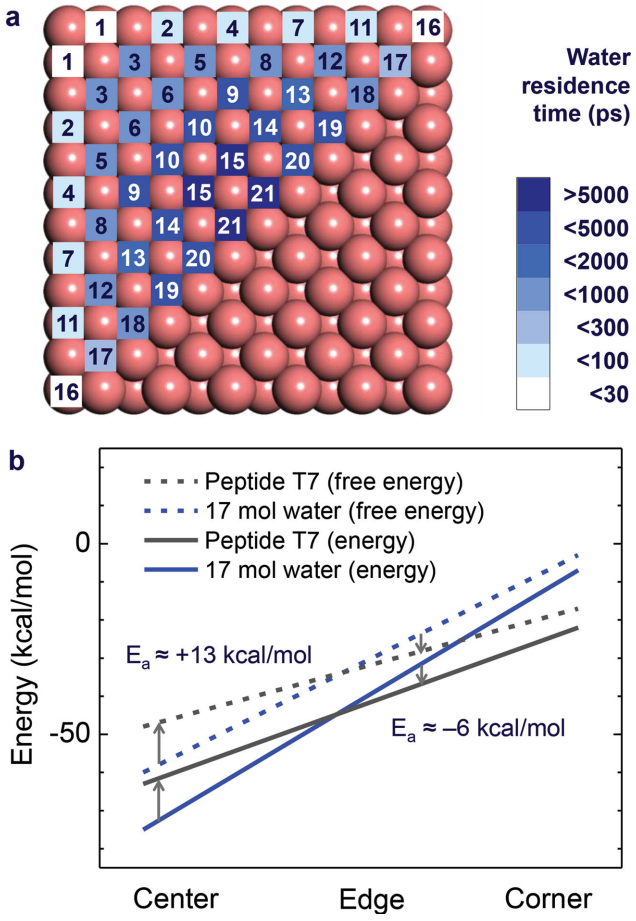

Figure 2. Local differences in the adsorption strength and mobility of water molecules on a cubic platinum nanocrystal of 2.35 nm side length and implications for the adsorption of peptide T7. a) Chemically distinct surface sites are identified by numerical labels. The average residence time describes how strongly a water molecule is adsorbed and how frequently it moves to a neighbor site or away into solution. Average residence times are more than two orders of magnitude higher at the center sites than at the corner sites. Adsorption to extended {100} surfaces is comparable to center portions of {100} facets. b) Schematic diagram of the spatially resolved binding energy and binding free energy for a fully extended peptide T7 as well as for 17 water molecules that compete for adsorption. The peptide is weaker bound compared to water in the center, resulting in desorption, and stronger bound than water near the edges and corners, resulting in adsorption at low concentration (energies are approximate).

cubic Pt nanoparticles out of more than one billion competing peptides at low concentration.[2]

The origin of the major difference between adsorption on nanocubes and repulsion on the extended {100} surface lays in the highly variable attraction of water and peptide molecules to spatially distinct surface portions of {100} facets of the cube (**Figure 2** and Figure S4, Supporting Information). The free energy of water adsorption is approximately –4 kcal mol^{-1} at the center of the facets and decreases to –0.6 kcal mol^{-1} at the corners. This difference by a factor of about six is several times larger than contributions by induced charges (Section S2.3, Supporting Information)[10] and results in major changes in water mobility. The average residence time of water molecules at the corners (Figure 2a, surface sites # 1, 2, 11, and 16) is over 100 times shorter than at the innermost sites (Figure 2a, surface sites # 15 and 21). Residence times at the center of the edges (Figure 2a, surface sites # 4 and 7) are more than ten times shorter than at the innermost sites (Figure 2a, surface sites # 15 and 21). In accordance, the energetically dominated strong attraction of about 17 water molecules, which could replace one fully bound peptide T7, prevents peptide adsorption near the center of {100} facets and on extended {100} surfaces (Figure 2b). The comparatively immobile, "multidentate" peptide T7, however, approaches the edges of {100} facets where the binding strength of water is low, enabling an extended conformation in which many polarizable atoms in the peptide attain close contact with epitaxial sites. The replaced water molecules (up to 17 per peptide T7) are then unbound and gain significant mobility (Figure 2b).

Therefore, selective adsorption of T7 on nanocubes, in contrast to repulsion on extended {100} surfaces, is associated with weaker binding of water near the edges and an optimum fit of T7 to epitaxial sites. The explanation is consistent with earlier observations of reduced binding of peptides and water at outer edges of stepped gold surfaces.[14] Spatial changes in binding free energy and mobility can apparently turn peptide repulsion into peptide attraction (for T7), which is a surprising yet thermodynamically logical outcome.

2.2. Specific Interactions of Single Peptides in Solution with Platinum Cuboctahedra

As a next step, the adsorption of a single peptide T7 on cuboctahedral seed crystals was analyzed in solution (Figure 1e,f). Seed crystals are formed upon fast nucleation during synthesis to grow into specific shapes (Section S4, Supporting Information).[2] 65% of the cuboctahedral surface consists of {100} facets and 35% of the surface is comprised of {111} facets. Time-averaged equilibrium binding configurations according to molecular dynamics simulations indicate direct contact of peptide T7 with both facets, whereby partial adsorption on {111} facets lowers the (negative) adsorption energy.

The comparison of extended {111} and {100} surfaces shows better epitaxial fit and much stronger attraction of peptide T7 to {111} surfaces (Figure S3, Supporting Information), as is also known for other peptide–metal combinations.[11,12,15,16] The reason for preferred adsorption onto extended {111} facets is the similarity of the geometry of sp^2 and sp^3 hybridized functional groups to the hexagonal pattern of epitaxial sites of 1.60 Å spacing. However, the finite size of the facets of small cuboctahedra alters the competition between peptide and water for adsorption (Figure 1e,f). A single peptide T7 spends about 65% of simulation time near the edge of {100} facets and 35% of time near the edge of {111} facets, similar to the contribution of these facets to the overall surface area and consistent with the stabilization of cuboctahedral geometry at low concentration in experiment (Section 2.4).

Further support for the computationally guided explanation of the selective binding mechanism of T7 to cubic nanocrystals comes from the observation of the binding specifics of peptide S7 to the same surfaces (Figure S5, Supporting Information).

Peptide S7 was selected against platinum {111} facets of octahedral nanoparticles using phage display, and generates a high yield of tetrahedral nanocrystals upon reductive synthesis independent of concentration.[2,20] In molecular dynamics simulation, slight repulsion of single S7 peptides on extended {100} surfaces and zero adsorption on {100} facets of cubes was found (Figure S5a–d, Supporting Information). The peptide displayed a weak preference toward edges of the cube when in direct contact with the surfaces. As expected from experiment, adsorption of S7 on the Pt cube is weaker than for T7, and S7 also coordinates a lower number of epitaxial sites with polarizable atoms (12 vs 20) (Figure S5c,d, Supporting Information). On cuboctahedra, S7 is strongly and almost exclusively bound to {111} facets with an adsorption energy of –32 kcal mol^{-1} (Figure S5e,f, Supporting Information). The significant difference between T7 and S7 peptides in experiment is equivalently seen in the simulation. Moreover, the role of phenylalanine in S7 and in a series of S7 mutants as a molecular switch that shifts the binding contrast in favor of {111} facets over {100} facets was previously demonstrated.[12,16,20]

2.3. Influence of Peptide Concentration on Facet Preference

As synthesis data will demonstrate in Section 2.4, facet recognition of peptide T7 also depends on the concentration in solution. Different concentrations lead to changes in peptide organization and adsorption strength on extended Pt {100} and Pt {111} surfaces (**Figure 3**). An increase in concentration is represented in molecular models by increased surface coverage from single to multiple peptides, whereby all peptide molecules can freely move from the surface into solution and vice versa. The two extended surfaces exhibit a large gap in adsorption preferences at low concentration that gradually diminishes as the surfaces become more peptidic rather than metallic at increased concentration (Figure 3a). In particular, self-assembly of multiple T7 peptides on the extended {100} surface was observed whereby specific peptide–peptide interactions turn overall repulsion of +13 kcal mol^{-1} at low concentration into overall attraction of –7 kcal mol^{-1} at high concentration (Figure 3a,b). A distinctive layer of water molecules between the surface and the peptides was thereby maintained. In comparison, the assembly of multiple T7 peptides in solution far away from the {100} surface lowered the energy only from approximately ±0 to –1 kcal mol^{-1} (Section S1.8, Supporting Information). The large difference in stabilization energy on the {100} surface confirms that the {100} surface specifically supports the assembly of T7 at higher concentration.

In contrast, the attraction per peptide T7 on the extended {111} surface diminishes at higher concentration (Figures 3a,3c, and S3, Supporting Information). Adsorption is strong at low concentration, however, the preference of T7 for flat-on attachment intensifies the competition for lateral space on the {111} surface upon increase in surface coverage and hinders full surface interaction of further peptides (Figure 3c). As a result, the attraction per peptide decreases at higher concentration. Stabilization of extended {111} and {100} surfaces by peptide T7 ultimately reaches a comparable level at high concentration (Figure 3a).

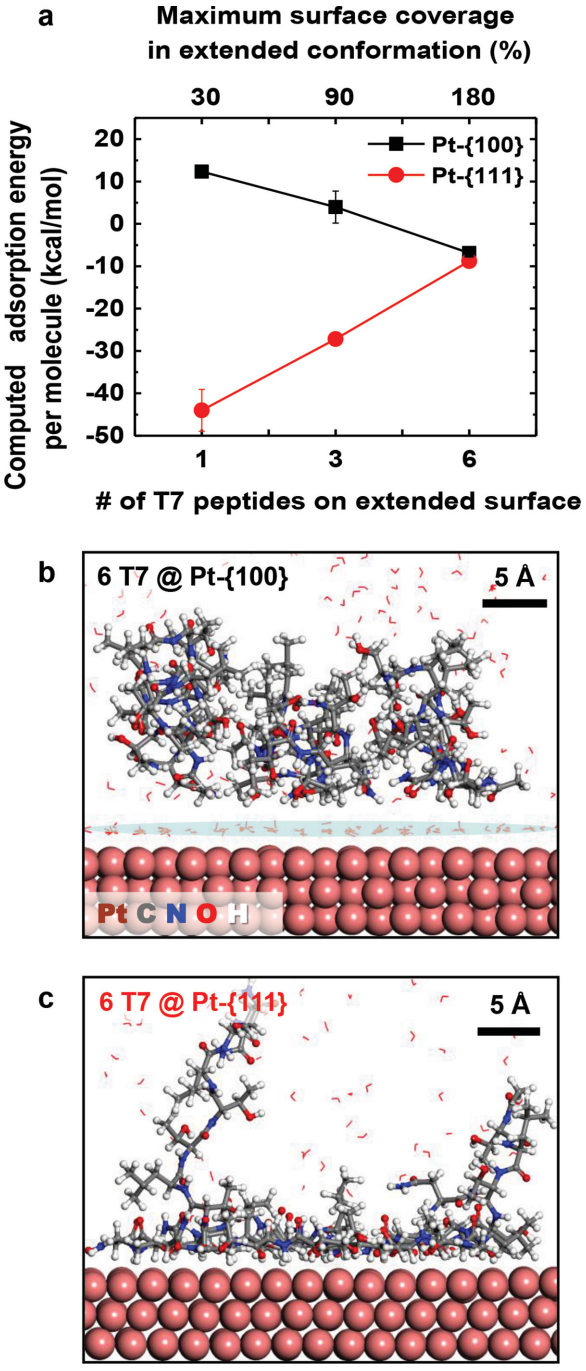

Figure 3. Concentration-dependent adsorption of T7 peptides on extended platinum {100} and {111} surfaces according to computation. a) Adsorption energy per molecule as a function of the number of molecules adsorbed. The top axis indicates the maximum possible surface coverage assuming extended conformations of all peptides. b,c) Representative snapshots illustrate binding configurations of multiple peptides and differences in binding mechanism on {100} and {111} surfaces, respectively.

Multiple S7 peptides do not stabilize Pt {100} surfaces at any concentration (Figure S6 and Section S1.8, Supporting Information). Repulsion from the {100} surface at low concentration and disintegration of S7 multilayers at high concentration are reflected in an increase in adsorption energies

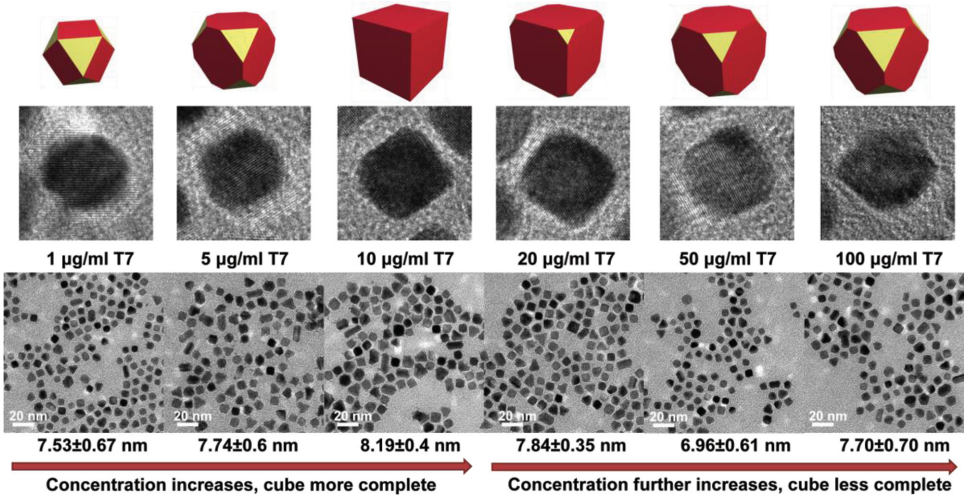

Figure 4. Shape development of T7-regulated platinum crystals at different concentration of T7. TEM and HRTEM images were recorded after completion of the reactions. Platinum nanocubes are more developed at moderate concentration of facet specific peptide (10–20 μg mL^{-1}) due to selective coverage of {100} facets (see also ref. [2]).

from +3 kcal mol^{-1} to +6 kcal mol^{-1} (Figure S6a,b, Supporting Information). In contrast to T7 peptides, Pt {100} surfaces thus promote dissolution of multiple S7 peptides. The association of multiple peptides S7 in solution was similarly unfavorable with an energy increase from approximately ±0 to +4 kcal mol^{-1} peptide (Section S1.8, Supporting Information). On the other hand, interactions of S7 with the {111} surface are very strong at low coverage and diminish as a function of concentration due to limited space for direct contact with the metal surface (Figure S6a and S6c, Supporting Information). S7 adsorption on the {111} surface yet remains about three times stronger compared to T7 at high coverage (–22 vs –7 kcal mol^{-1}). These differences between S7 and T7 illustrate the specific properties of T7 as a stabilizer of {100} surfaces at increased concentration in contrast to the strong attraction of S7 to {111} surfaces as observed in experiment.[2,20] The critical role of concentration for specific adsorption of peptides T7 and S7 is also consistent with earlier studies that showed the choice of ligands as well as the influence of the molar ratio of ligands to metal precursor to be decisive factors for the observed geometry and size of metal nanocrystals.[6,8] The results demonstrate that facet-specific self-organization of ligands and binding differentials for various {h k l} facets can be probed using all-atom molecular dynamics simulation in a very good agreement with experiment for various concentrations.

2.4. Formation of Cubes from Cuboctahedral Seed Crystals

The bio-mediated synthesis of platinum nanocrystals from soluble precursors begins with fast nucleation upon injection of a strong reducing agent, which results in the formation of cuboctahedron seeds of ≈2 nm size.[2] Subsequent reduction of platinum precursor using a mild reducing agent facilitates slower growth of nanocrystals by adatom deposition while the presence of peptides regulates the shape evolution (Section S4, Supporting Information). As time progresses, in the presence of peptide T7, cuboctahedron seeds grow to 7–8 nm size and the shape changes from cuboctahedron to cube and cube-like particles (**Figure 4**).[2] The principal mechanism involves growth by adatom deposition and facet-specific retardation of growth by adsorbed peptides, which is experimentally supported for this[2] and similar systems.[4–7,20,33] An alternative growth mechanism could be cluster attachment, however, the then expected twinned and elongated structures were not observed.[34]

As described in Section 2.2, the surface of a cuboctahedron seed consists of {100} and {111} facets that occupy approximately 65% and 35% of the total surface area, respectively. A facet-specific ligand could then preferentially cover one type of facets, biasing atom deposition towards the less stabilized facet and achieving shape control. In experiment, facet selectivity was observed to be sensitive to the concentration of T7 peptide. Thereby, platinum nanocubes were more developed at moderate concentration of T7 (10–20 μg mL^{-1}) while they were less developed at lower and higher peptide concentration (Figure 4). The maximum yield of cube and defective cube-like structures bounded by {100} facets was about 60% (Figure S7 and Section S4, Supporting Information). The size of cubes produced at intermediate concentration was also slightly larger than that of the other cuboctahedra-like structures at low and high concentration. Consequently, the laboratory data suggest an influence of the concentration of peptide T7 on the yield as well as on the size of cubic nanocrystals.

Molecular dynamics simulations at low concentration of T7 support the stabilization of cuboctahedra (Section 2.2) and further simulations at increasing T7 concentration consistently explain the experimental observations (**Figure 5**). A suitable indicator of the final shape was found to be the equilibrium location of peptide T7 on {100} and {111} facets of cuboctahedral seed crystals, which serve as a start structure to develop into cubes. Preferential binding of peptides to either facet causes a deviation from the natural 65:35 ratio and facilitates kinetically controlled growth of distinct nanocrystal shapes. Specifically, when more than 65% of peptide T7 is located on {100} facets, it is said to stabilize {100} facets and lead to the formation of cubes. Vice versa, when more than 35% of peptide

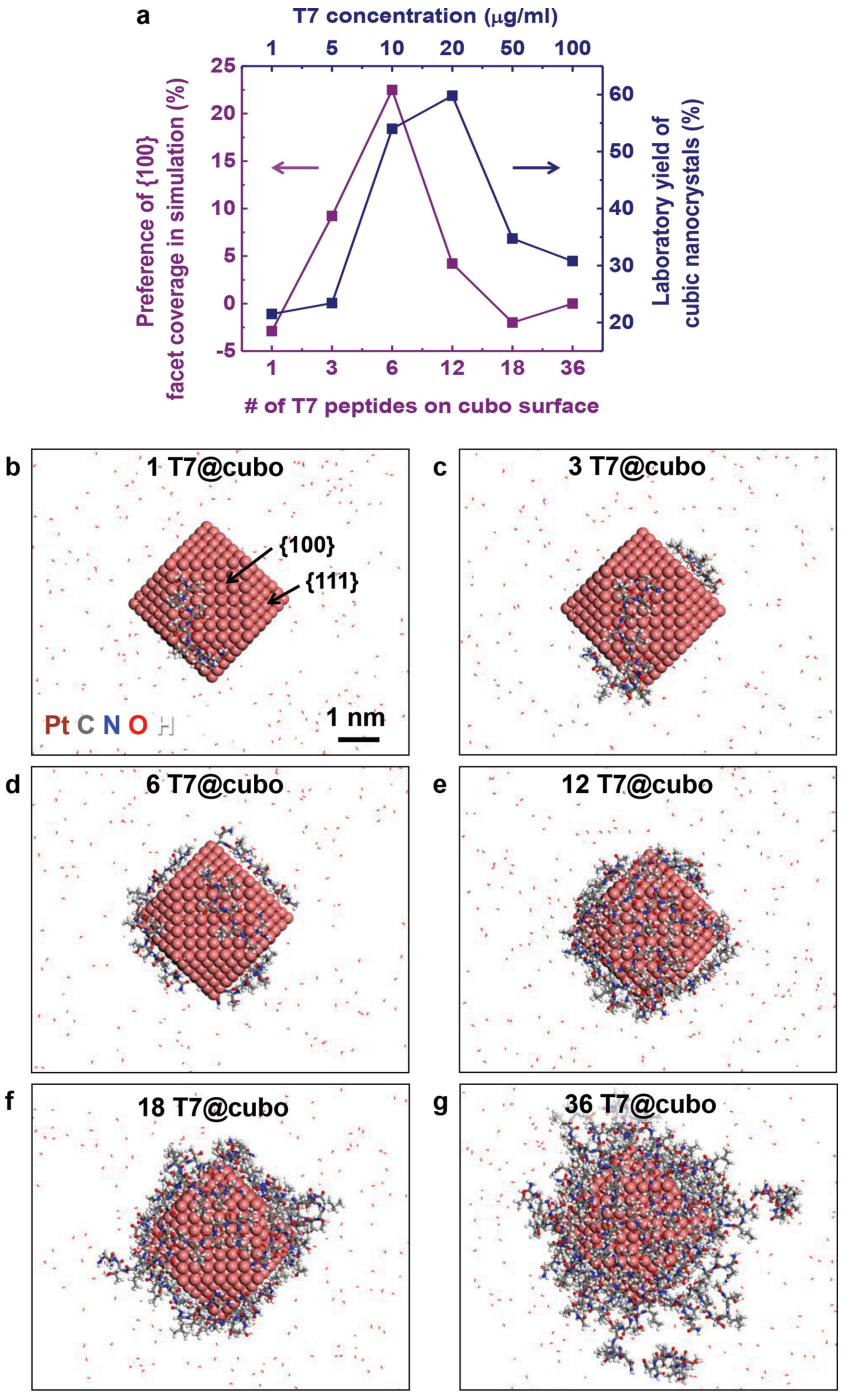

Figure 5. Preference of the T7 peptide toward coverage of {100} facets at intermediate concentration leads to relatively higher growth rate of {111} facets and formation of cubic nanoparticles. a) Correlation of the yield of cubic nanocrystals as a function of T7 concentration in experiment with the binding preference toward {100} facets as a function of surface coverage in the simulation. b–g) Representative snapshots show the binding configuration of T7 and the relative coverage of {100} and {111} facets for different concentration. Adsorption–desorption equilibria are seen at higher surface coverage.

T7 is located on {111} facets, different {111} bounded shapes may be obtained (tetrahedra, octahedra). Therefore, the coverage of facets (**Figure 6**), the normalized coverage of facets (Figure S8, Supporting Information) as well as the difference in normalized coverage of {100} and {111} facets (Figure 5a) were monitored. The peptides were initially set free to locate on either facet of the cuboctahedral seeds in the simulation. Independent start structures, multiple replicas, and advanced equilibration techniques allowed the precise analysis of time-averaged locations of peptides on the crystal facets (Sections S1.3, S1.4, and S1.9, Supporting Information).

A critical quantity is thereby the number of molecules adsorbed onto the nanocrystal surface for a given concentration of peptide T7 in solution (Figure 5a). The precise relationship between concentration in solution and surface coverage during nanostructure nucleation and growth can still not be determined by imaging, scattering, and spectroscopy techniques. The data would also be difficult to obtain from simulations due to high demands on system size and simulation time. Nevertheless, the relation between concentration and surface coverage was estimated semiquantitatively according to known concentrations of peptide and metal precursor, scattering, and AFM data (Section S1.10, Supporting Information).[2,29,35] The surface coverage for a given peptide concentration in Figure 5a (i) represents system-specific data, (ii) reflects the trend of increasing adsorption at higher concentration, and (iii) covers the possible range of surface coverage from 0 to ≈300% corresponding to the lower and upper limits of relevance.[35]

The simulation results then show that the spatial distribution of peptide T7 on {100} and {111} facets (Figure 5, Figure S8, Supporting Information) indeed changes as a function of concentration. The same is true for the facet distribution of S7 peptides (Figure 6, Figure S9, Supporting Information). The relative coverage of {100} and {111} facets with T7 peptides remains close to the native 65:35 ratio of a cuboctahedron for most concentrations, and exceeds 65% on {100} facets at intermediate concentration in favor of the formation of cubes (Figures 5a, 6a, S8, Supporting Information). A distinct increase occurs at about 6 T7 that correlates with a maximum yield of cubic nanocrystals in experiment, given some uncertainty in the exact number of peptides on the surface. The preference towards {100} facets enables faster growth in the {111} directions and slower growth in the {100} direction by adatom deposition to complete cubic shapes observed by HRTEM (Figure 4). Binding configurations and relative coverage of {100} and {111} facets also show that below the optimal concentration of T7 not enough peptide would be

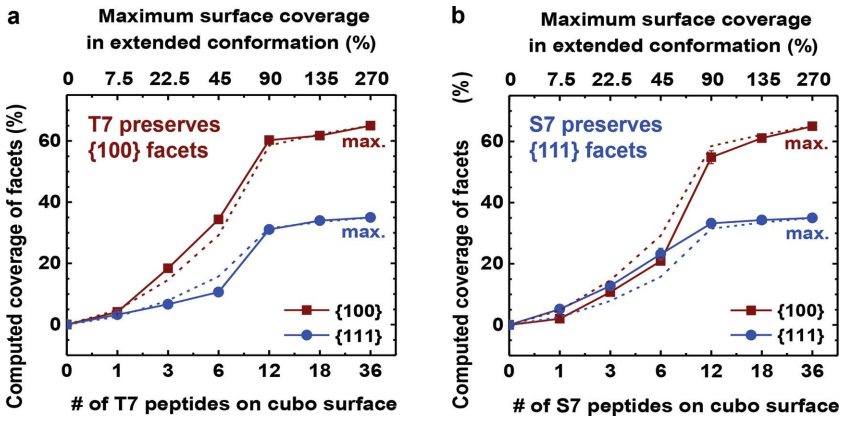

Figure 6. Facet preferences of T7 and S7 peptides on cuboctahedral seed crystals according to simulation. Solid lines represent the coverage with peptides and dotted lines represent the geometric contribution of facets. a) A minor preference of T7 to {100} facets at intermediate surface coverage is seen, consistent with a limited yield of cubes. b) A major preference of S7 to {111} facets across a wide range of surface coverage is observed, consistent with a high yield of {111} bounded nanocrystals (e.g., tetrahedra).

available to stabilize all six {100} facets of cuboctahedron seeds, leading to less developed shapes (Figure 5b). At high concentration and high coverage, both types of facets are about equally covered and the binding preference to the {100} facet is eventually lost (Figure 5f,g). Particle growth would then occur in {111} and {100} directions at about the same rate, confirmed in synthesis by the preference toward smaller cuboctahedral nanocrystals rather than cubes (Figure 4). An optimal concentration of T7 between 10–20 μg mL^{-1}, corresponding to about 40%–90% effective surface coverage, is therefore suggested to result in the highest yield of cubic nanocrystals (Figures 4,5).

In addition to the shape of the nanocrystals as a function of concentration, the size was found to vary between slightly smaller cuboctahedra at low and high peptide concentration compared to larger cubes at intermediate concentration (Figure 4). While the nanocrystal shape is determined by the *relative* growth rate of {100} versus {111} facets, the nanocrystal size is determined by the *absolute* growth rates of {111} and {100} planes and thus affected by the adsorption strength of the peptide. Simulation indicates weaker average adsorption of T7 to the cube at intermediate concentration (6 T7) than at lower and at higher concentration (Figure S10a, Supporting Information). Faster adatom deposition could be achieved at weaker peptide adsorption, leading to larger nanocrystal size upon completion as is observed for the cubes. Therefore, the average nanocrystal size measured in TEM shows a trend consistent with the average computed adsorption energy towards cubes (Figure S10a, Supporting Information).

Limitations in the yield of cubic nanocrystals to 60% are also notable (Figure 4 and Figure S7, Supporting Information). When the preference of T7 peptides to {100} facets (Figure 6a) is compared to that of S7 peptides to {111} facets (Figure 6b), the excess coverage of {100} facets by T7 is found to be comparatively small and concentration dependent. In contrast, a high excess coverage of {111} facets by S7 peptides is found across a wide range of concentration. These differences are consistent with a limited yield and a limited definition of the cubes (Figure 4 and Figure S7, Supporting Information). In contrast, peptide S7 yields more than 70% tetrahedra with less defects.[2,20] Therefore, the extent of facet preference observed in the simulation also correlates with the trend in experimentally observed nanocrystal yield.

2.5. Comparison to Nanocrystals Regulated by Peptide S7 and Thermodynamic Stability

Therefore, the analysis of the selectivity of other peptides such as S7 towards specific facets on growing cuboctahedra adds valuable insight for comparison. Peptide S7 exhibits a strong bias to {111} facets for a wide range of low to high concentration (Figure 6b and S9, Supporting Information). At low and intermediate concentration, {111} portions of the cuboctahedron surface attract more than 50% of S7 peptides, far above the native 35:65 ratio between {111} and {100} facets. The preference of S7 peptides towards {111} facets also continues up to high concentration (≥18 S7). Therefore, in excellent correlation with experimental observations, S7 peptides facilitate faster growth in the {100} direction by adatom deposition and support the formation of {111} bounded tetrahedron or octahedron particles with only weak dependence on concentration (Figures 6b and S9, Supporting Information).[2,20] The larger differential in facet preference explains a higher yield of tetrahedra and cuboctahedra (>70%) (Figure 6), and the larger negative adsorption energy on cuboctahedra (Figure S10b, Supporting Information) rationalizes a smaller nanoparticle size (6 nm) in comparison to cubes grown in the presence of peptide T7 (≈60% yield and 8 nm size).

Moreover, adsorption energies from molecular dynamics simulations help understand the thermodynamic stability of cuboctahedra and nanocubes in more detail (Figures S10, Supporting Information). Adsorption energies of peptide T7 below zero indicate stabilization of cuboctahedra and nanocubes once they are formed (Figures S10a, 5b–g and S11a–f, Supporting Information). The negative adsorption energy of a single T7 on nanocubes in comparison to peptide S7 (and potential other peptides) also agrees with the initial selection of T7 peptides against cubic nanoparticles by phage display. S7, on the other hand, stabilizes cuboctahedral crystals far better than cubes at any concentration owed to stronger adsorption onto {111} facets (Figures S10b, S9c–h, and S11g–l, Supporting Information).

2.6. Summary of Emerging Simulation Capabilities

The foregoing discussion shows that preferences of shape, yield, and size of metal nanocrystals can be explained on the basis of experimental data and atomistic simulations using models of real-size nanocrystals in contact with ligands (**Table 1**). A key role is thereby attributed to facet-specific binding of ligands at various concentrations in aqueous solution, which can be monitored via molecular dynamics simulations with the CHARMM-INTERFACE force field (Section S2, Supporting

Table 1. Emerging capabilities of atomistic simulations with the CHARMM-INTERFACE force field to predict ligand binding to metal nanocrystals and rationalize growth preferences in aqueous solution at the 1 nm to 100 nm scale (this work and refs.[4,10,13–16,22,25,27,29].)

Calculated property	Relation to experiment
Selectivity of peptides to extended and finite-size nanocrystal {h k l} facets	Identification of facet specific peptides using phage display
Facet coverage and preferences in facet coverage on nanocrystals	Shape and yield of nanocrystals (HRTEM)
Binding free energies of peptides	Binding constants and size of nanocrystals
Spatial location of peptides on {h k l} facets and average distance of residues from the surface	Atomic-level information, EXAFS, IR/ Raman spectroscopy
Above properties as a function of the number of peptides on the surface	Above properties as a function of peptide concentration and surface coverage
Spatially and temporally resolved trends in peptide assembly on nanocrystal surfaces	Atomic-level information, QCM, in situ measurements

Information).[13,15] The force field currently covers the metals Al, Ag, Au, Cu, Ni, Pb, Pd, and Pt in the absence of thin oxide layers, i.e., under reductive conditions, and any biological and organic ligands included in the CHARMM force field. Other force fields such as OPLS, AMBER, PCFF, and GROMACS can also be used with the same extension for fcc metals.[13] Since information on facet preferences, superficial peptide assembly, and binding energies remains difficult to obtain from laboratory measurements, the computational methods introduce opportunities to support the design of new materials at the 1 to 100 nm scale. Recently, also reactive extensions have been developed.[25,29] Alternative computational tools are currently not available, for example, quantum-mechanical methods cannot be employed at this scale due to prohibitive computational cost and mesoscale simulation methods would exclude essential chemical details.

Specifically, atomistic simulations can accomplish (1) the analysis of ligand selectivity to various {h k l} facets and to full-size nanoparticles, (2) the analysis of preferences in coverage of facets and of the spatial location of ligands, (3) the computation of binding free energies, (4) the analysis of the concentration dependence of the above properties, and (5) dynamic monitoring of ligand assembly on nanoparticle surfaces (Table 1). The accuracy is often quantitative and comparisons to a range of laboratory observations can be made, including phage display, nanocrystal shape and yield in HRTEM, nanocrystal size and ligand binding constants, EXAFS data on coordination numbers, monitoring of molecular assembly using quartz crystal microbalances (QCM), as well as in-situ techniques.

3. Conclusions

Binding mechanisms of single and multiple peptides T7 and S7 to even metal surfaces and nanocrystals have been explained in atomic-level detail consistent with data from phage display. Observations in synthesis, HRTEM, and molecular simulation suggest that growth from cuboctahedral platinum seed crystals to nanocubes involves adatom deposition and peptide T7 thereby slows down crystal growth in the {100} direction depending on concentration.

Specific binding of single peptides T7 on cubic platinum nanocrystals occurs preferentially near the edges rather than at inner portions of {100} facets as a result of substantially reduced binding of water at the edges. Water at the edges is therefore more mobile, and this entropic advantage in combination with a high degree of fit of peptide T7 to {100} epitaxial sites enables weak peptide binding. In contrast, water binding dominates over peptide binding at the center of {100} facets.

The peptide concentration was found to strongly affect the binding strength on extended surfaces as well as on nanocrystal facets. Higher concentration of T7 peptides on an extended {100} surface, for example, turned repulsion into attraction while S7 peptides were not attracted to {100} facets at any concentration and strongly prefer {111} facets. In molecular models, differences in peptide concentration were represented by progressive changes in surface coverage.

The yield of cubic nanocrystals in reductive synthesis showed a major dependence on peptide concentration as well, including a pronounced maximum at intermediate concentration of peptide T7. Experimental observations of shape and yield could be correlated with concentration-dependent changes in coverage of competing facets on cuboctahedral seed crystals in molecular dynamics simulation. When the coverage of {100} facets by the peptide exceeds the percentage of {100} surface facets of bare cuboctahedra (65%), growth is favored on the {111} facets and increases the laboratory yield of cubic nanocrystals in correlation with the extent of facet preference in the simulation. The observed relative size of nanocrystals showed additional correlations with the computed adsorption energy per peptide (stronger adsorption corresponds to smaller size). The suggested mechanism of adatom growth, modulated by changes in peptide binding to the bounding facets of seed crystals, agrees with further observations for a tetrahedra-forming peptide S7, prior experimental observations,[2,4–7,33,34] and previously derived design rules for facet-specific ligands.[15]

Therefore, simulations with the CHARMM-INTERFACE force field (the extended version of the CHARMM-METAL force field) offer new insight into facet-selective ligand binding and growth preferences of nanocrystals in atomic resolution. Such computational guidance can increasingly complement trial-and-error based experimental approaches to accelerate synthesis and characterization of metal nanostructures on the 1 to 100 nm scale. Future work could provide quantitative details for a wide range of systems and possibly incorporate kinetic events in the simulation.

4. Experimental Section

Large-scale atomistic molecular dynamics simulations were carried out using the CHARMM-INTERFACE force field, the NAMD program, effective equilibration and sampling techniques, as well as novel analysis protocols (Sections S1 and S2, Supporting Information). Time–temperature equivalence (annealing) and multiple parallel replicas were employed to collect thoroughly weighted structural and thermodynamic ensemble averages. The analysis of data from molecular dynamics simulations focused on the spatial location and binding energies of the peptides on the nanocrystal surfaces as a function of surface coverage to establish correlations with experimentally observed preferences in

nanocrystal shape, yield, and size. A new protocol is reported to analyze the time-average facet coverage with peptides during MD simulations (Section S1.9, Supporting Information).

Computed adsorption energies and adsorption free energies of the peptides in aqueous solution are approximately equal for the short 7-mer peptides (within 10%), as previously verified for similar systems.[14,36] Thereby, the loss in translational and conformational entropy upon adsorption of the peptides is compensated, or slightly overcompensated, by the gain in mobility of surface-released water molecules (Figure 2b, Table S1, and Section S1.6, Supporting Information). Uncertainties in computed adsorption energies are typically ±10% or ±1 kcal mol^{-1}, whichever the greater.

Peptides T7 and S7 were synthesized according to the fmoc solid phase peptide synthesis protocol using a CS 336X synthesizer (C S Bio), characterized by Liquid Chromatography/Mass Spectrometry (LC/MS), purified, and confirmed to be of >90% purity with valid masses before usage (Section S3, Supporting Information). Acyl and amide groups at the N and C termini protected both peptides, respectively, to eliminate pH sensitive ionic groups. Molecular models of the peptides were also chosen charge neutral with the same protecting groups. The peptides remained charge neutral across a wide range of pH, including 7.5 during phage display and 5.5–6.0 in nanocrystal synthesis.

Pt nanocrystals were synthesized by reduction of H_2PtCl_6 precursor using a strong reducing agent ($NaBH_4$) to induce nucleation, followed by a weak reducing agent (ascorbic acid) to sustain growth in the presence of peptides at different concentration. The nanocrystals were then characterized by HRTEM to analyze shape, size, and yield (Section S4, Supporting Information).

Interactions of the peptides with extended metal surfaces and nanocrystals (>1.5 nm size) in aqueous solution are predominantly noncovalent. Localized chemical bonds are negligible, as shown in prior work on platinum-binding peptides[2,3,20] and other precious-metal binding ligands.[4,14–16,23,24,31,37] Thiol groups with known covalent bonding character to metals are absent.[29] Contributions to adsorption by induced charges are negligible due to the absence of ionic groups in the end-protected peptides, consistent with data for ligands with different density of ionic groups (Section S2.3, Supporting Information).[10,27]

Supporting Information

Supporting Information is available from the Wiley Online Library or from the author.

Acknowledgments

H.R. and H.H. acknowledge support from the National Science Foundation (award DMR 0955071), the Air Force Research Laboratory (AFRL and UES, Inc.), and the University of Akron. L.R. and Y.H. acknowledge support from the Office of Naval Research (ONR) (award N00014–08–1–0985), the Army Research Office (ARO) (award 54709-MS-PCS), and the Sloan Research Fellowship. H.H. and Y.H. further acknowledge support from the National Science Foundation (award DMR 1437355). L.Y.R. and Y.H. also acknowledge the Electron Imaging Center of Nanomachines for TEM support and Y. T. for LC-MS support. H.R. and H.H. acknowledge the allocation of computing resources at the Ohio Supercomputer Center.

Received: November 21, 2014
Published online: January 21, 2015

[1] a) R. Coppage, J. M. Slocik, M. Sethi, D. B. Pacardo, R. R. Naik, M. R. Knecht, *Angew. Chem.-Int. Ed.* **2010**, *49*, 3767; b) R. Coppage, J. M. Slocik, B. D. Briggs, A. I. Frenkel, R. R. Naik, M. R. Knecht, *ACS Nano* **2012**, *6*, 1625; c) Z. F. Kuang, S. N. Kim, W. J. Crookes-Goodson, B. L. Farmer, R. R. Naik, *ACS Nano* **2010**, *4*, 452; d) J. M. Slocik, J. S. Zabinski, D. M. Phillips, R. R. Naik, *Small* **2008**, *4*, 548; e) D. Vanmaekelbergh, *Nat. Nanotechnol.* **2009**, *4*, 475; f) I. Lee, R. Morales, M. A. Albiter, F. Zaera, *Proc. Natl. Acad. Sci. U.S.A.* **2008**, *105*, 15241; g) H. F. Qian, Y. Zhu, R. C. Jin, *Proc. Natl. Acad. Sci. U.S.A.* **2012**, *109*, 696; h) G. A. Somorjai, Y. M. Li, *Proc. Natl. Acad. Sci. U.S.A.* **2011**, *108*, 917; i) L. D. Zarzar, B. S. Swartzentruber, J. C. Harper, D. R. Dunphy, C. J. Brinker, J. Aizenberg, B. Kaehr, *J. Am. Chem. Soc.* **2012**, *134*, 4007.

[2] C. Y. Chiu, Y. J. Li, L. Y. Ruan, X. C. Ye, C. B. Murray, Y. Huang, *Nat. Chem.* **2011**, *3*, 393.

[3] a) L. Y. Ruan, C. Y. Chiu, Y. J. Li, Y. Huang, *Nano Lett.* **2011**, *11*, 3040; b) C. Y. Chiu, Y. J. Li, Y. Huang, *Nanoscale* **2010**, *2*, 927.

[4] R. Coppage, J. M. Slocik, B. D. Briggs, A. I. Frenkel, H. Heinz, R. R. Naik, M. R. Knecht, *J. Am. Chem. Soc.* **2011**, *133*, 12346.

[5] J. M. Petroski, Z. L. Wang, T. C. Green, M. A. El-Sayed, *J. Phys. Chem. B* **1998**, *102*, 3316.

[6] a) Y. Xia, Y. Xiong, B. Lim, S. E. Skrabalak, *Angew. Chem.-Int. Ed.* **2009**, *48*, 60; b) B. Lim, M. Jiang, J. Tao, P. H. C. Camargo, Y. Zhu, Y. Xia, *Adv. Funct. Mater.* **2009**, *19*, 189.

[7] Y. Yin, A. P. Alivisatos, *Nature* **2005**, *437*, 664.

[8] T. S. Ahmadi, Z. L. Wang, T. C. Green, A. Henglein, M. A. ElSayed, *Science* **1996**, *272*, 1924.

[9] a) M. P. Allen, D. J. Tildesley, *Computer Simulation of Liquids*, Clarendon Press, Oxford **1987**; b) H. Heinz, *J. Comput. Chem.* **2010**, *31*, 1564; c) L. Duchesne, G. Wells, D. G. Fernig, S. A. Harris, R. Levy, *ChemBioChem* **2008**, *9*, 2127; d) V. Petkov, B. N. Wanjala, R. Loukrakpam, J. Luo, L. Yang, C.-J. Zhong, S. Shastri, *Nano Lett.* **2012**, *12*, 4289; e) G. C. Schatz, *Proc. Natl. Acad. Sci. U.S.A.* **2007**, *104*, 6885; f) S. V. Patwardhan, F. S. Emami, R. J. Berry, S. E. Jones, R. R. Naik, O. Deschaume, H. Heinz, C. C. Perry, *J. Am. Chem. Soc.* **2012**, *134*, 6244; g) P. Schravendijk, N. van der Vegt, L. Delle Site, K. Kremer, *ChemPhysChem* **2005**, *6*, 1866; h) J. Schneider, L. C. Ciacchi, *J. Am. Chem. Soc.* **2012**, *134*, 2407; i) L. Delle Site, C. Abrams, A. Alavi, K. Kremer, *Phys Rev. Lett.* **2002**, *89*, 156103; j) L. B. Wright, P. M. Rodger, T. R. Walsh, S. Corni, *J. Phys. Chem. C* **2013**, *117*, 24292; k) N. A. Vellore, J. A. Yancey, G. Collier, R. A. Latour, S. J. Stuart, *Langmuir* **2010**, *26*, 7396; l) R. R. Netz, D. Andelman, *Phys. Rep.* **2003**, *380*, 1.

[10] H. Heinz, K. C. Jha, J. Luettmer-Strathmann, B. L. Farmer, R. R. Naik, *J. R. Soc. Interface* **2011**, *8*, 220.

[11] R. B. Pandey, H. Heinz, J. Feng, B. L. Farmer, J. M. Slocik, L. F. Drummy, R. R. Naik, *Phys. Chem. Chem. Phys.* **2009**, *11*, 1989.

[12] J. Yu, M. L. Becker, G. A. Carri, *Small* **2010**, *6*, 2242.

[13] H. Heinz, R. A. Vaia, B. L. Farmer, R. R. Naik, *J. Phys. Chem. C* **2008**, *112*, 17281.

[14] J. Feng, J. M. Slocik, M. Sarikaya, R. R. Naik, B. L. Farmer, H. Heinz, *Small* **2012**, *8*, 1049.

[15] J. Feng, R. B. Pandey, R. J. Berry, B. L. Farmer, R. R. Naik, H. Heinz, *Soft Matter* **2011**, *7*, 2113.

[16] H. Heinz, B. L. Farmer, R. B. Pandey, J. M. Slocik, S. S. Patnaik, R. Pachter, R. R. Naik, *J. Am. Chem. Soc.* **2009**, *131*, 9704.

[17] G. Cicero, A. Calzolari, S. Corni, A. Catellani, *J. Phys. Chem. Lett.* **2011**, *2*, 2582.

[18] S. Corni, M. Hnilova, C. Tamerler, M. Sarikaya, *J. Phys. Chem. C* **2013**, *117*, 16990.

[19] L. B. Wright, P. M. Rodger, S. Corni, T. R. Walsh, *J. Chem. Theory Comput.* **2013**, *9*, 1616.

[20] L. Ruan, H. Ramezani-Dakhel, C.-Y. Chiu, E. Zhu, Y. Li, H. Heinz, Y. Huang, *Nano Lett.* **2013**, *13*, 840.

[21] a) L. L. Atanasoska, J. C. Buchholz, G. A. Somorjai, *Surface Sci.* **1978**, *72*, 189; b) L. E. Firment, G. A. Somorjai, *J. Chem. Phys.* **1977**, *66*, 2901.

[22] H. Heinz, T.-J. Lin, R. K. Mishra, F. S. Emami, *Langmuir* **2013**, *29*, 1754.
[23] S. H. D. Lacerda, J. J. Park, C. Meuse, D. Pristinski, M. L. Becker, A. Karim, J. F. Douglas, *ACS Nano* **2010**, *4*, 365.
[24] J. M. Slocik, R. R. Naik, *Adv. Mater.* **2006**, *18*, 1988.
[25] H. Ramezani-Dakhel, P. A. Mirau, R. R. Naik, M. R. Knecht, H. Heinz, *Phys. Chem. Chem. Phys.* **2013**, *15*, 5488.
[26] M. Hnilova, E. E. Oren, U. O. Seker, B. R. Wilson, S. Collino, J. S. Evans, C. Tamerler, M. Sarikaya, *Langmuir* **2008**, *24*, 12440.
[27] K. C. Jha, H. Liu, M. R. Bockstaller, H. Heinz, *J. Phys. Chem. C* **2013**, *117*, 25969.
[28] W. Jiang, B. Y. Kim, J. T. Rutka, W. C. Chan, *Nat. Nanotechnol.* **2008**, *3*, 145.
[29] R. Coppage, J. M. Slocik, H. Ramezani-Dakhel, N. M. Bedford, H. Heinz, R. R. Naik, M. R. Knecht, *J. Am. Chem. Soc.* **2013**, *135*, 11048.
[30] a) R. R. Naik, S. E. Jones, C. J. Murray, J. C. McAuliffe, R. A. Vaia, M. O. Stone, *Adv. Funct. Mater.* **2004**, *14*, 25; b) M. Sarikaya, C. Tamerler, A. K. Y. Jen, K. Schulten, F. Baneux, *Nat. Mater.* **2003**, *2*, 577.
[31] J. M. Slocik, M. O. Stone, R. R. Naik, *Small* **2005**, *1*, 1048.
[32] G. van Anders, N. K. Ahmed, R. Smith, M. Engel, S. C. Glotzer, *ACS Nano* **2014**, *8*, 931.
[33] C. Y. Chiu, L. Ruan, Y. Huang, *Chem. Soc. Rev.* **2013**, *42*, 2512.
[34] L. Y. Ruan, H. Ramezani-Dakhel, C. Lee, Y. J. Li, X. F. Duan, H. Heinz, Y. Huang, *ACS Nano* **2014**, *8*, 6934.
[35] C. Tamerler, E. E. Oren, M. Duman, E. Venkatasubramanian, M. Sarikaya, *Langmuir* **2006**, *22*, 7712.
[36] a) *Bio-Inspired Nanotechnology: From Surface Analysis to Applications*, Springer, New York **2014**, Chapter 2; b) F. S. Emami, V. Puddu, R. J. Berry, V. Varshney, S. V. Patwardhan, C. C. Perry, H. Heinz, *Chem. Mater.* **2014**, *26*, 5725.
[37] X. Fu, Y. Wang, L. Huang, Y. Sha, L. Gui, L. Lai, Y. Tang, *Adv. Mater.* **2003**, *15*, 902.